Surfactant Diffusion into Lysozyme Crystal Matrices Investigated by Quantitative Fluorescence Microscopy

O. D. Velev, E. W. Kaler, and A. M. Lenhoff*

Center for Molecular and Engineering Thermodynamics, Department of Chemical Engineering, University of Delaware, Newark, Delaware 19716

Received: February 1, 2000; In Final Form: July 5, 2000

Small quantities of ionic surfactants modify the crystallization of lysozyme and lead to the formation of phases with different morphologies. By using fluorescent probes, we demonstrate that the surfactants are incorporated into the growing crystals (which is a possible reason for crystal twinning) and can penetrate and adsorb within previously formed crystals. To characterize the interactions and the mass transfer of surfactants inside the crystalline protein matrices, we studied the infusion of lysozyme crystals with pyrene-based fluorescent surfactants by quantitative fluorescence microscopy. The fluorescence intensity data were fitted to the diffusion equation to obtain the effective diffusion coefficient of the fluorophore in the crystals. The diffusion coefficients obtained range from 2×10^{-10} to 30×10^{-10} cm^2/s, depending on the type and size of the surfactant. The slow infusion is a consequence of the strong surfactant adsorption on the protein lattice; the estimated energy of adsorption is 10−12 *kT*. Fluorescence recovery after photobleaching (FRAP) experiments with saturated crystals showed that surfactant self-diffusion in these crystals is negligible, which is yet another indication of strong adsorption. The data shed light on the interactions between condensed protein phases and surfactants and are relevant to protein purification and crystallization and to the manipulation of proteins by light.

Introduction

Crystallization is used in separation and purification of proteins and is a necessary precursor to the characterization of their three-dimensional structure by X-ray diffraction. The major factor controlling the crystallization is the molecular interaction between the protein molecules.[1,2] Measuring and adjusting the balance of attraction and repulsion between the molecules, as characterized by the osmotic second virial coefficient, can lead to predictable crystallization conditions.[2,3] However, the mechanism of molecular action of many common crystallization additives is still unclear. One particular class of such additives is surfactants,[4] which are known to bind to proteins in solution,[5,6] and in larger quantities, to cause their denaturation.[6] Small amounts of nonionic surfactants may improve the quality of crystals formed from soluble proteins,[7] but under other conditions can cause precipitation by modification of the protein−protein interactions.[5,6,8,9] We have found that the presence of small quantities of anionic surfactants can drastically modify the morphologies of protein crystalline phases.[9] Both the continuum properties and the molecular mechanisms of surfactant action during protein crystallization are, however, poorly characterized. For instance, it has not been determined whether the surfactant affects the dynamics of nucleation and/or growth, the phase equilibrium of the intact crystal, or both. Questions at the molecular level include whether the surfactant molecules are held immobile within the crystal structure, if they remain free in the crystal, or if they are expelled after crystallization.

Here we report data on the interaction between surfactants and crystalline protein, analysis of which provides qualitative and quantitative answers to several of these questions. The measurements provide estimates of the rates and time scales of surfactant diffusion inside the protein matrix, as well as estimates of the energy of interaction between the surfactant and the crystalline protein. These measurements are extended to molecular-level events by probing how the behavior of the surfactants is affected by the type and size of their hydrophobic and hydrophilic portions.

We used as model surfactants fluorescent pyrene derivatives having both hydrophilic and hydrophobic portions. The amphiphilic properties of these molecules should make them reasonably good models for widely used conventional surface-active agents. The concentrations and fluxes of the pyrene-based amphiphiles can be traced by fluorescence microscopy. Hen egg white lysozyme crystals, which can be obtained easily and reproducibly, and the properties and morphology of which are well-known, were used as substrates for surfactant infusion.

In the Results section, we first present the quantitative fluorescence measurements on the rate of surfactant infusion into nonfluorescent crystals, interpreted in terms of a classical diffusion model. The second part of the Results section describes the outcome of fluorescence recovery after photobleaching (FRAP) experiments aimed at evaluating the self-diffusion coefficient of the surfactant in the crystals. The results are discussed from the perspective of surfactant−crystal interactions and their relevance to practical protein crystallization and purification, and to potential applications of protein crystals in materials science and drug delivery.

Materials and Methods

Materials. Lysozyme was obtained from Sigma (prod. no. L-6876). The lyophilized protein was dissolved in a solution containing 0.3 M NaCl, 3×10^{-4} M citrate buffer and 10 mg/L NaN_3. The pH of the protein solutions was adjusted by adding

* Author for correspondence. E-mail: lenhoff@che.udel.edu. Phone: (302) 831 8989. Fax: (302) 831 4466.

10.1021/jp000393o CCC: $19.00
Published on Web 09/13/2000

TABLE 1: Summary of the Pyrene Derivatives Used as Surfactants in This Work

surfactant name	side chain	surfactant code
1-pyrenesulfonic acid, sodium salt	$-SO_3^-Na^+$	P-80
1-pyrenecarboxylic acid	$-COOH$	P-146
1-pyrenebutanoic acid	$-C_3H_6COOH$	P-1903
1-pyrenehexanoic acid	$-C_5H_{10}COOH$	P-3840
1-pyrenepropylamine hydrochloride	$-C_3H_6NH_3^+Cl^-$	P-6254

small amounts of 1 M HCl and NaOH. The solutions were filtered both before and after protein dissolution using Anotop (USA) inorganic syringe filters with cutoff values of 20 and 100 nm, respectively. The protein concentrations were 15 mg/mL for solutions adjusted to pH 10 and 25 mg/mL for solutions at pH 6.5. The crystals were grown by a batch method, in which the protein solutions were left at 4 °C for 3−14 days in closed glass or plastic vials. Nucleation was sometimes enhanced by seeding with a few crystals from previously crystallized samples.

The fluorescent pyrene compounds were supplied by Molecular Probes (USA) and were used without further purification. All of the fluorescent markers are 1-pyrene derivatives that differ only in the type and size of the side chain; Table 1 shows the structures and the manufacturer codes. These compounds have highly hydrophobic moieties and so have rather low solubilities.

Methods. An Olympus BH-2 fluorescence microscope equipped with a 100 W stabilized mercury lamp was used. The samples were excited in the 334−365 nm range and the light emitted above 410 nm was collected and analyzed. The digital images were collected by a cooled, high-sensitivity, linear response CCD camera (Star-1, Photometrics, Inc.) and transferred to a computer. A scientific software package (IPLab Spectrum for Macintosh) was used for frame processing.

The samples for the experiments were encapsulated in 1 mm thick Probe-clip imaging chambers from Sigma. A few droplets of the lysozyme solutions along with a few suspended crystals were transferred by sterile pipet to the chamber, placed with the polycarbonate side down. A minute amount of the crystalline fluorescent substance (≈0.1−0.5 mg per mL of crystalline suspension) was gently scattered in the solution. The samples were immediately sealed from above by 0.17 mm thick microscope cover slips and transferred onto the microscope stage for observation. To ensure the hermetic seal of the small chambers, a thin layer of viscous fluorinated grease (Krytox, DuPont, USA) was applied between the silicon resin surface and the cover glass.

In the microscopy experiments, a large, uniformly shaped protein crystal was selected and its dimensions were measured in transmitted illumination. The thickness of the crystal was measured by focusing a 40× objective onto the crystal top and onto the bottom successively and reading the difference from the microscope stage micrometric screw. Observation was then continued in fluorescence mode to obtain the intensity profiles across the crystal in time. Digital images were stored at increasing time intervals for up to 48 h. None of the sealed samples exhibited evaporation or bacterial growth during the observation period.

To estimate the solubility via the fluorescence intensity of the surfactants, surfactant slurries were prepared in electrolyte/buffer solution and left to equilibrate for 4 h. Liquid samples were then filtered and transferred to tightly capped 1 cm path length quartz cuvettes. The fluorescence spectra were recorded on an SLM 8100 spectrofluorimeter (SLM Aminco, USA), with excitation at 340 nm and emission integrated over the range from 360 to 410 nm. All spectra, obtained in 2−4 successive emission scans, were stable and reproducible.

Results

Initial Infusion of Nonfluorescent Crystals. The lysozyme amino acid sequence includes six tryptophan residues, which are fluorescent in the UV region below 400 nm when excited at wavelengths up to 300 nm.[10] The component of UV light at these wavelengths in the microscope illuminator was very low, and the barrier filter used cuts off all light below 400 nm. Preliminary tests showed that the original lysozyme crystals in their mother liquor appeared totally dark and no background could be attributed to intrinsic protein fluorescence. However, when a small amount of pyrene derivative was added into the chamber with the lysozyme crystals, the crystals began to exhibit fluorescence within 10−30 min due to adsorption of the surfactant on the protein lattice. The crystals became brightly fluorescent within a period of 24−48 h or more, as the surfactant had penetrated the crystals and distributed uniformly throughout their bulk (Figure 1a).

We were also able to create brightly fluorescent crystals by crystallizing lysozyme at pH 7 in solutions of 0.5 M NaCl in the presence of P-80 (sulfonic acid derivative). Initially some aggregation and precipitation were noticed in these samples, but after 7−10 days crystals had grown out of the precipitate. Not only were these crystals very bright against the relatively dark background, but their appearance and morphology were often different from the regular needlelike orthorhombic crystals obtained in the absence of surfactant (Figure 1b). These simple experimental observations lead to a number of important conclusions: (i) the surfactants used have a strong affinity for lysozyme and bind to the crystals, rendering them fluorescent, (ii) the surfactants accumulate in the crystals rather than being excluded during their growth, (iii) the accumulation of the pyrene derivatives in the growing protein phase can change the crystal morphology, as observed with other surfactants,[9] and (iv) accumulation of the pyrenes or other surfactants can also occur via infusion after crystal growth.

The case where the surfactant penetrates preformed nonfluorescent crystals was studied quantitatively by following the distribution of the fluorescence intensity across a large crystal with time. Most of the experiments were carried out with needlelike lysozyme crystals obtained at pH 10. These crystals have orthorhombic symmetry and grow as long thin needles with an approximately rectangular cross-section.[3,11] After samples of these crystals were sealed in the microscopic chamber in the presence of pyrene surfactant, their fluorescence intensity increased with time (Figure 2), and a nonequilibrium diffusion profile across the crystal was observed, in which the edges were brighter than the interior of the crystals. When the crystals had become saturated with surfactant (after ca. 24 h), the intensity reached a plateau, and the distribution profile became more uniform.

To extract quantitative data from the fluorescent profiles, digital pictures of a single crystal being infused with fluorophore were recorded at intervals typically starting at 15 min and gradually increasing to 1−2 h. The intensity profiles across the crystal (i.e., vertically in Figure 2) were extracted from the data. The overall procedure for data reduction and correction is schematically illustrated in Figure 3. To minimize noise, the values from vertical arrays 10−30 pixels wide were read and then collapsed into a one-dimensional sequence by averaging the values from the pixels in each row. As the intensity of the crystal fluorescence increased, so did the background illumination due to scattering in the surrounding solution and reflection from the cell bottom. To correct for the background illumination, the data from a 20−50 pixel long background patch well outside the

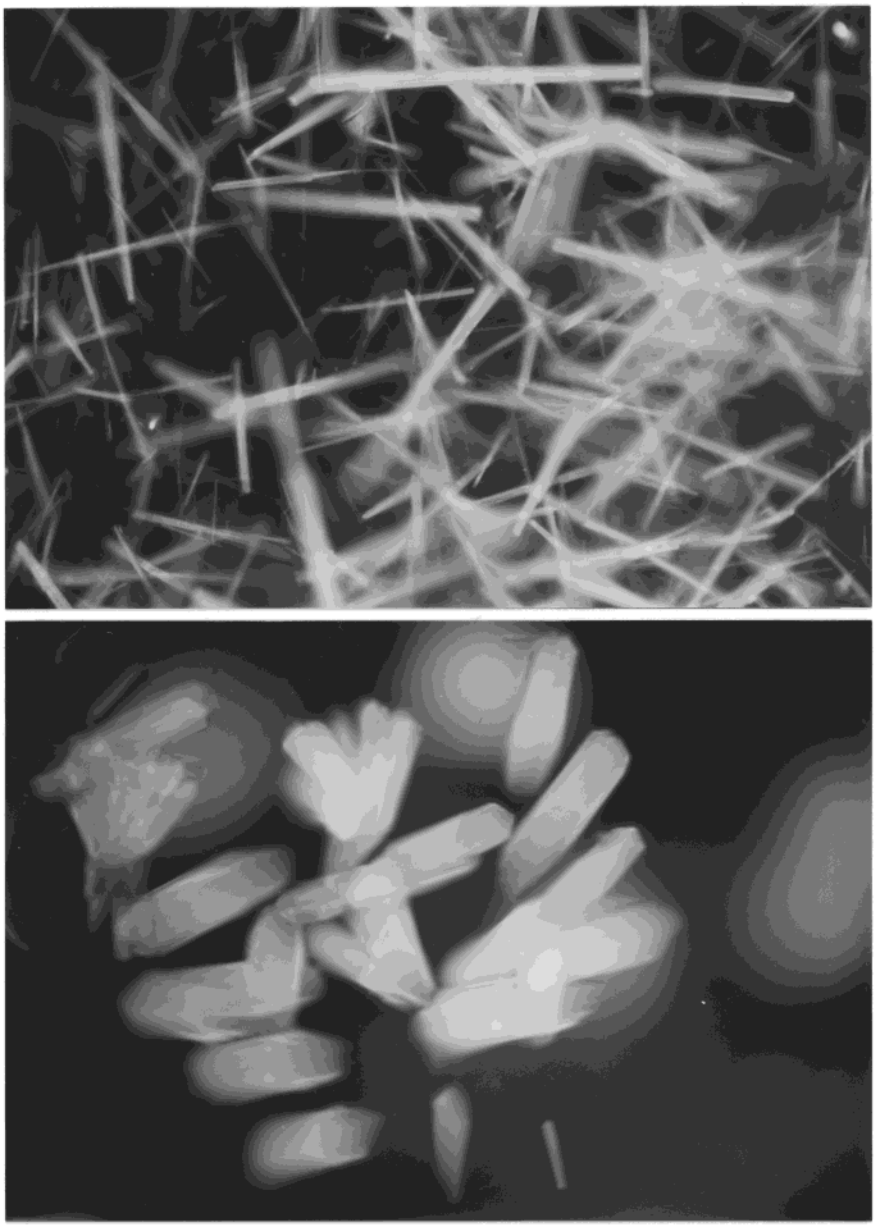

Figure 1. Micrographs of fluorescent lysozyme crystals in 0.3 M electrolyte and at pH 10 obtained via surfactant infusion: (a) needlelike orthorhombic crystals infused with surfactant; (b) chunky crystals of unknown symmetry obtained when lysozyme is crystallized in the presence of the fluorophore.

crystal were averaged, and the number obtained was subtracted from each point of the intensity profile. In principle, one can also correct for the nonuniform field illumination of the excitation light from the microscope source, but our experience has shown that this correction is negligible in the vertical direction.

A typical full set of corrected intensity data obtained during the infusion of a crystal with P-80 is shown in Figure 4. Not only does the intensity increase with time, but the distribution profile changes, exhibiting a minimum in the center of the crystal area that increases in depth until ca. 120 min, and then levels off. The intensity at 24 h is uniform, with the exception of the large peak on the right-hand side. Independent experiments showed that this peak is caused by refraction of light at the inclined crystal edge and is therefore an optical artifact not related to the actual accumulation of surfactant. As the infusion from the two halves of the crystal should be symmetric, only data collected from the other half of the crystal were used in the numerical calculations.

Analyzing the uptake measurements requires clarification of the nature of the quantitative information that is captured by the microscope camera. The 10× N.A. 0.40 objective used has relatively low vertical resolution, so features ± 10 μm from the focal plane appear approximately in focus. Fluorescent objects at a distance of at least 3 times this value will contribute to the measured intensity. Thus, the objective takes an optical cross section at least 60 μm deep, which is on the order of the crystal thickness (30−70 μm), so the results represent a cumulative measurement of the fluorescence emission from the full depth of the crystal. A second point concerns the surfactant flux into the crystal across the exposed faces. It may seem that no flux would enter the protein crystal from below, i.e., through the face resting on the cell floor. However, the cell bottom is covered with protein debris and neither the wall nor the crystal is ideally flat, so there is a fluid layer between the crystal and the wall. We assume that layer to be thick enough to allow essentially unretarded transport to the lower crystal face.

The cumulative effect of these assumptions is that the surfactant infuses into the crystal from all four sides, with the data representing a vertical optical cut through the full crystal. More direct evidence that the crystal is indeed infused from all

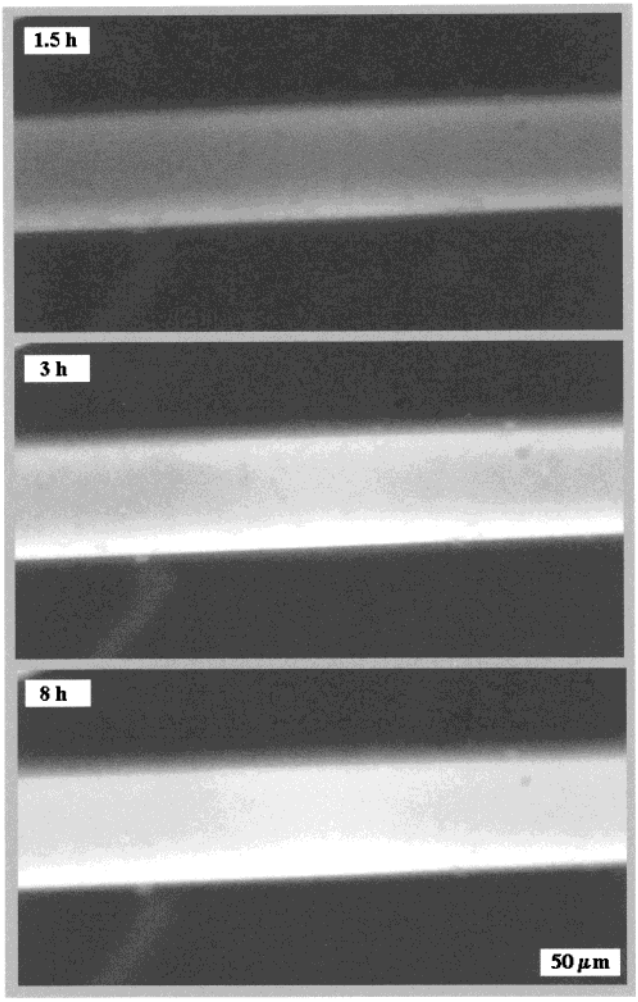

Figure 2. Successive pictures of initially nonfluorescent lysozyme crystal being infused with pyrene sulfonate (P-80). Note the change of the magnitude and distribution of intensity with time.

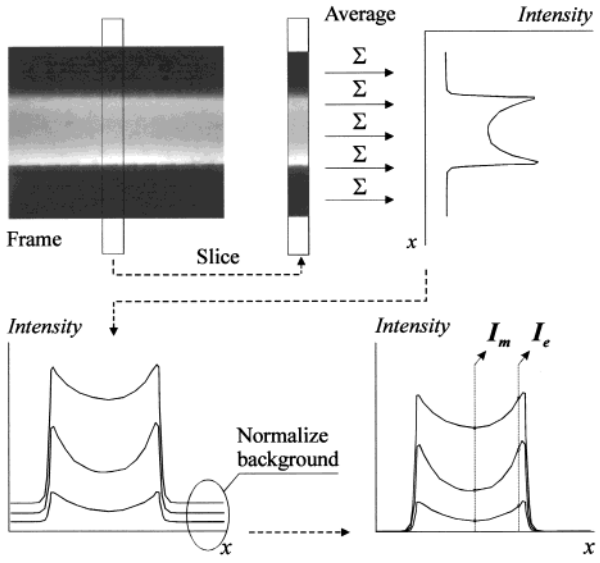

Figure 3. Schematic of the procedure for reducing and correcting the image data from the CCD camera.

four sides is provided by a procedure that allows the diffusion profiles to be replicated into etched areas that can be observed by regular bright field microscopy.[12] In brief, while the crystal is subjected to the surfactant flux, it is illuminated though the microscope by a strong light beam that leads to denaturation of

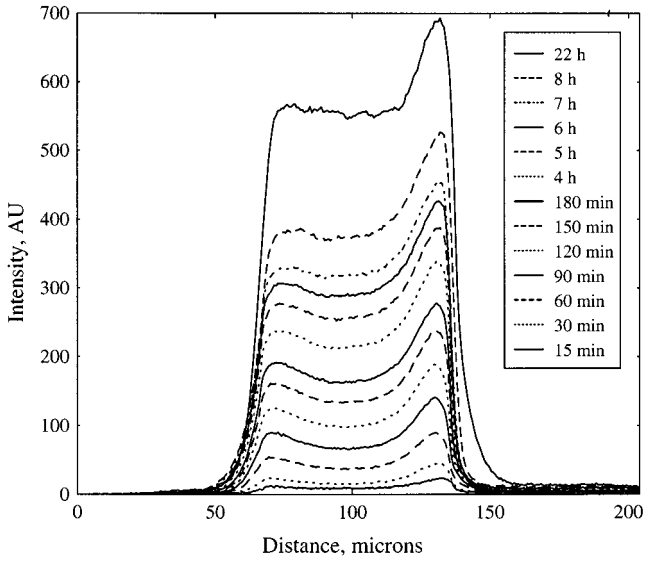

Figure 4. Fluorescence intensity curves vs time for the infusion of an orthorhombic crystal with P-80.

the protein in the crystal areas where the surfactant has accumulated. This results in etching of the crystal in the surfactant-infused areas. The procedure has interesting implications for materials science, as described in detail elsewhere,[12] but here it suffices to show the results of such optical etching of a crystal that was infused with P-1903 (butanoic acid derivative) for 12 h and then bleached (Figure 5). The crystal has suffered damage on all four faces, which clearly shows that infusion occurred through all of them, and the resulting fluorescence is visible in the objective light path.

The diffusion model used to fit the data takes into account the fluxes through all four faces of the crystal, as shown in Figure 6. Diffusion within the crystal is assumed to occur only in the interstitial volume, with the free solution diffusion coefficient D_s reduced by the effects of the finite interstitial volume, as well as by hindrance and tortuosity effects,[13] to a value D_h. This interstitial diffusion is also coupled to surfactant adsorption, yielding the overall diffusion equation[14]

$$\epsilon\frac{\partial C}{\partial t}+\frac{\partial q}{\partial t}=D_h\nabla^2 C \qquad (1)$$

where C is the local interstitial concentration (per unit interstitial volume), q is the concentration of adsorbed surfactant (per total crystal volume), and ϵ is the void fraction of the crystal. If adsorption equilibrium applies locally within the crystal, which is reasonable in view of the short lateral diffusion distances involved, q is related to C by an adsorption isotherm. At relatively low surfactant concentrations, conditions that apply to most of our experiments (see later), this relationship may be assumed to be linear, i.e., $q = KC$, which yields from eq 1 an equation in the form of the simple diffusion equation:

$$\frac{\partial C}{\partial t}=D_e\nabla^2 C \qquad (2)$$

However, the diffusion parameter here is the effective diffusion coefficient, D_e, defined as[14]

$$D_e=\frac{D_h}{\epsilon+K\Phi} \qquad (3)$$

where Φ is the specific surface area available for adsorption. The strong adsorption characteristics give rise to large values

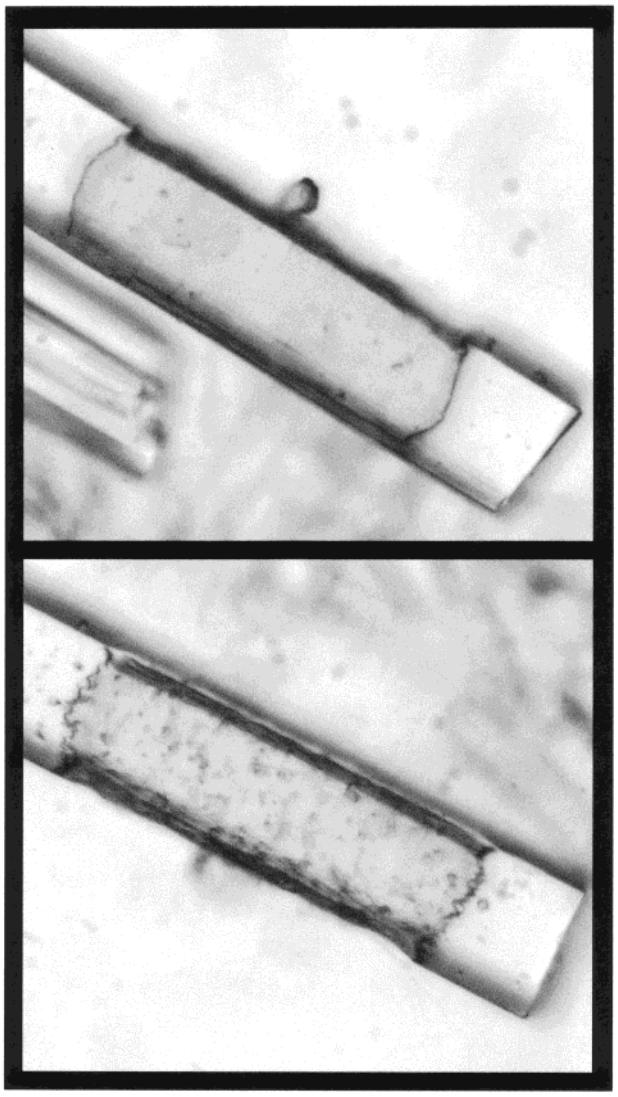

Figure 5. Micrographs of faces of a crystal that has been partially infused with P-1903 and then etched by a strong beam of light from the microscope objective. The grooves correspond to the areas penetrated by the surfactant prior to photodestruction. Note the uniform etching from all four sides of the crystal.

of K and hence strong attenuation of the effective diffusion rate, and by determining D_e from our data we can estimate the strength of adsorption. The boundary condition used at all solvent-crystal interfaces is

$$D_h \frac{\partial C}{\partial n} = k(C_0 - C) \qquad (4)$$

where n is the local outwardly directed normal to the crystal face. C_0 is the surfactant concentration in the surrounding solution, which can be adequately represented by the solubility, and k is the mass transfer coefficient for surfactant transport to the crystal surface. Additional boundary conditions are provided by the symmetry that applies at the center of the crystal.

The principal model parameter to be determined is the effective diffusion coefficient of the surfactant, D_e, which will allow the value of K to be estimated from eq 3. In seeking to determine D_e, however, it is also necessary to estimate k. In addition, the concentration scale C_0 must be related to the experimentally accessible quantity, the fluorescence intensity, or else the model and data must be compared in dimensionless form. In either case, comparison of experiment and theory

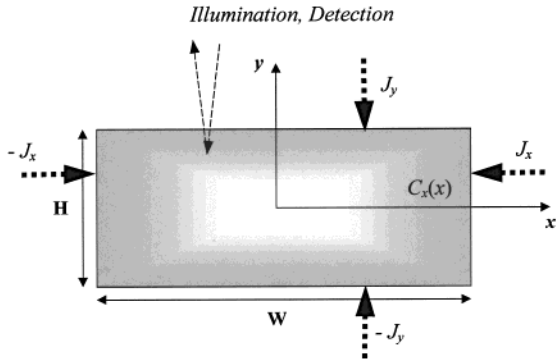

Figure 6. Schematic of the diffusion model, showing the geometric parameters.

requires the problem defined by eqs 2 and 4 to be solved within the rectangular cross section of the crystal, but the inhomogeneity of boundary condition eq 4 precludes an analytical solution.[15] Instead, we decompose the problem by expressing the measured intensity $I(x,t)$ as

$$I(x,t) = \Gamma\left[HC_x(x,t) + 2\int_0^t [-J_y(y{=}H/2,t)]\,dt\right] \qquad (5)$$

where Γ relates the interstitial fluorophore concentration C to the intensity measured by the camera. $C_x(x,t)$ is the contribution to the concentration profile due to horizontally diffusing surfactant entering the crystal through the sides (Figure 6), which causes the nonuniform intensity across the crystal. The integral, on the other hand, is of the vertical flux $J_y(t)$ of surfactant, assumed to be uniform across the top and bottom surfaces of the crystal and thus causing the steady increase in the overall observed intensity.

The key to the decomposition is that the two contributions to infusion occur on different time scales. The characteristic time for diffusion inside the crystal can be estimated in terms of the adsorption-adjusted diffusion coefficient D_e and the crystal thickness H as H^2/D_e. Crystal saturation, on the other hand, is on an even longer time scale, of order KH/k, because of the additional transport resistance within the surrounding solution, and this controls the overall increase in intensity. Because of this latter resistance, $C \ll C_0$ during the early stages of the experiment, so that eq 4 suggests that a limiting approximation applies in which the infusion flux reaches a constant value of kC_0, which should result in a linear increase in overall intensity[15,16] corresponding to the slope dI/dt of the intensity plot.

The data (Figure 7a) indeed suggest that a steady state is reached in the shape of the concentration profile after the transient period of initial infusion, with saturation approached at long times. In the constant-flux approximation, the intensity difference between the border and the midplane of the crystal, $\Delta I = I_e - I_m$, should become roughly constant as a function of time. This difference is independent of mass transfer outside the crystal and allows the diffusion coefficient, D_e, to be estimated via the time-independent approximate solution to the 1-D transport problem

$$D_e = \frac{H^2}{8\Delta I}\frac{dI}{dt} \qquad (6)$$

This calculation procedure allows very simple data processing as the averaged values are merely substituted into the above equation. The data for Pyr-SO_3Na (Figures 4 and 7a) show that an approximately steady state is reached and maintained after

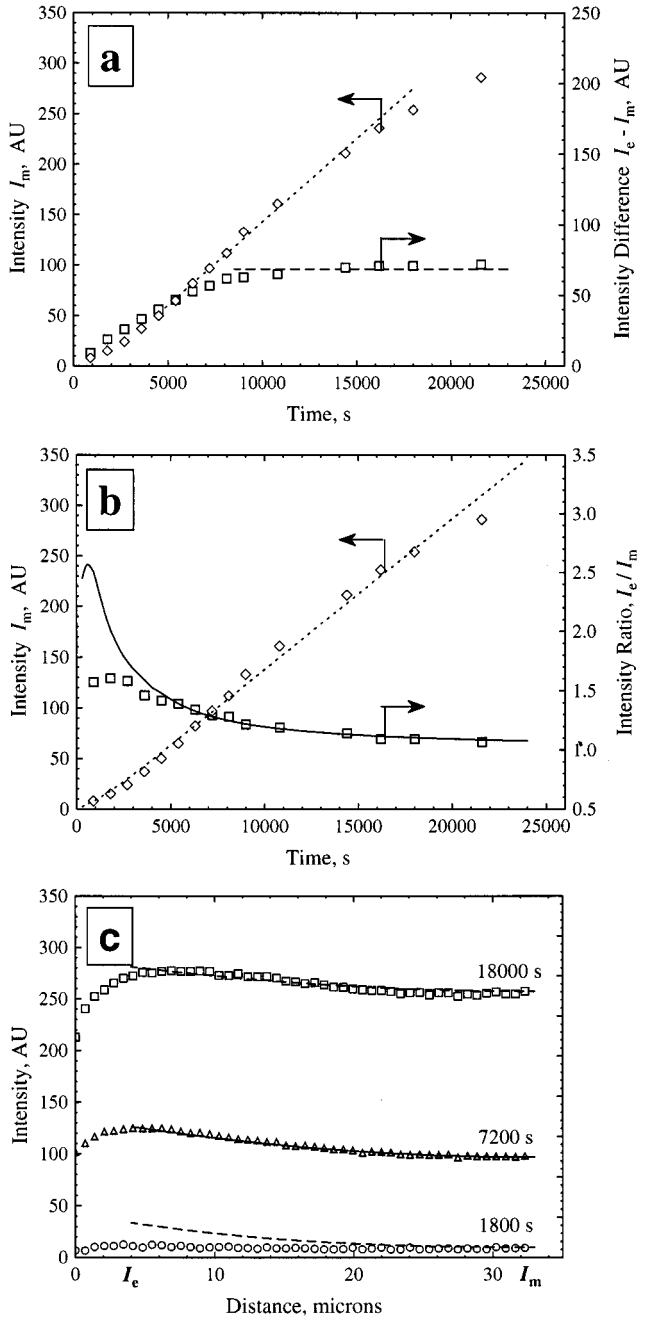

Figure 7. Examples of the fits of the infusion data and model tests in crystals infused with P-80: (a) constant-flux approximation—estimates based on the linear portions of the ΔI and the intensity in the middle of the crystal, $I_m(t)$; (b) fits of I_m and the intensity ratio I_e/I_m based on the full solution of the one-dimensional diffusion problem; (c) some reconstructed intensity profiles on the basis of the two-point fit compared to the actual data. Symbols, experimental; lines, theory.

120 min. Calculations by the above formula yield an estimated value of $D_e = 10.8 \times 10^{-10}$ cm^2/s.

We also estimated the parameters more directly from the full solution to the one-dimensional diffusion problem. The data fitted to obtain the values of D_e were the intensity in the middle of the crystal, I_m, and the ratio of the intensities at the crystal border and middle, I_e/I_m, both as a function of time. I_m depends mainly on external transport and I_e/I_m predominantly on internal transport, allowing the parameters to be determined largely independently again. To avoid experimental artifacts at the edges of the crystal, the intensity I_e was not measured exactly at the edges, but a small distance (3−10 μm) away from them (Figure 3). An example of the fit obtained is shown in Figure 7b. Although the model shows some deviation from the data points, particularly at short times, an acceptable fit of a complex data set is obtained. The deviations at short times may be explained in part by the low signal-to-noise ratio of the very weakly fluorescent crystals, which also hinders precise focusing, as well as by deviations from the model idealizations. The diffusion coefficient in this case is estimated to be 10.5×10^{-10} cm^2/s, in good agreement with the value from the first procedure.

Both procedures thus allow D_e and kC_0 to be obtained largely independently, but do not allow k and C_0 to be separated directly. k depends on the surfactant diffusion coefficient in free solution and, more importantly, on the location of the surfactant crystals relative to that of the protein crystals; a value of order D_s/H would be expected. C_0, on the other hand, reflects more clearly just the surfactant solubility, although surfactant−protein interactions in solution may play a role as well. The two factors can be separated in principle by estimating C_0 via spectrofluorimetric measurements of the emission intensity of saturated protein-free surfactant solutions. These values, normalized by the values for Pyr-C_3COOH, are shown in Table 2 and can be compared to the kC_0 values. As expected, both parameters follow the same general trends. However, a complete correlation between the two sets of data is not possible, due to variations in the aperture alignment, light intensity, and distance between the protein crystals and the fluorophore grains in the different fluorescence microscope experiments.

The reliability of the model and the experimental reproducibility were verified in a number of different ways. To check the reproducibility of the data, a second experiment with a newly prepared batch of P-80 was carried out with a crystal of different dimensions. A satisfactory match of the data with the model was obtained without changing the values of D_e and kC_0. We also checked how the model reconstructs the whole intensity profile across the crystal based on fitting the intensity only at the center of the crystal and near the edge. A typical result of such a test is shown in Figure 7c. While there is deviation from the modeled data at short times as expected, the overall description is satisfactory.

In order to compare the effects of the surfactant side chain, the infusion of each of the surfactants into orthorhombic crystals at pH 10 was measured. A few infusion experiments were also carried out with tetragonal lysozyme crystals at pH 6.5 to estimate the effect of the protein packing and charge density. The results are summarized in Table 2. In general the effective surfactant diffusion coefficients obtained are 3−4 orders of magnitude lower than those of the corresponding free molecules in water (estimated to be 4.3×10^{-6} cm^2/s based on literature data[17]). These diffusion coefficients are sensitive to the molecular weight and the charge state of the surfactant, decreasing with increasing surfactant molecular weight. The protein crystal form and the pH have a major impact on the diffusion coefficients, with infusion of the crystals at pH 6.5 5−10 times faster than at pH 10.

This retardation results from coupling of the surfactant diffusion to adsorption on the lysozyme in the crystal, as discussed earlier. To obtain the value of K (and the energy of adsorption) from the effective diffusion coefficients given in Table 2, one also needs an estimate of the parameter Φ in eq 3. The volumes of the unit cells in the orthorhombic and tetragonal lysozyme crystals are available from the Brookhaven Protein Data Bank.[18] After dividing the volume by the number of molecules in a unit cell, the values of 30 845 Å^3/molecule for the orthorhombic and 29642 Å^3/molecule for the tetragonal, or a common approximation of 3.0×10^4 Å^3/molecule, are

TABLE 2: Parameters Estimated from Experimental Data Using the Diffusion Model[a]

surfactant	crystal type	effective diff coeff, $cm^2/s \times 10^{10}$	E_{ads}, kT units	normalized I_0	normalized I_0 in satd soln
Pyr-SO_3Na	orthorhombic at pH 10	10.5	10.6	0.94	26.0
Pyr-COOH	orthorhombic at pH 10	13.6	10.3	4.5	9.30
Pyr-C_3COOH	orthorhombic at pH 10	4.62	11.4	1.00	1.00
Pyr-C_5COOH	orthorhombic at pH 10	4.6	11.4	0.041	0.007
Pyr-C_3NH_3Cl	orthorhombic at pH 10	2.1	12.2	1.59	1.89
Pyr-C_3COOH	tetragonal at pH 6.5	18	10	2.15	0.036
Pyr-C_3NH_3Cl	tetragonal at pH 6.5	28.5	9.6	5.44	1.09

[a] The last column gives the normalized fluorescence intensity of saturated surfactant solutions in the absence of protein. The estimated, or measured, error is within ±2 digits of the last reported digit.

obtained. This value is then used to determine K from eq 3, which we do by assuming D_h to be the free-solution diffusion coefficient. This neglects hindrance and tortuosity effects, but since these are unlikely to attenuate diffusion by more than an order of magnitude, the values of K estimated should not be significantly overestimated.

The adsorption constant K can be interpreted in terms of binding energy by approximating it as

$$K = B \exp\left(-\frac{E_{ads}}{kT}\right) \quad (7)$$

where E_{ads} is the energy of adsorption, k the Boltzmann constant, T the temperature, and B a preexponential factor that can be approximated by the range of the intermolecular interactions ≈1 Å. The values obtained are shown in the fourth column of Table 2, with all of the values on the order of 10 kT units. Although these values might be reduced by 1−2 kT if hindrance and tortuosity were accounted for as discussed above, the strength of adsorption of the fluorophore molecules onto the protein lattice remains significant.

FRAP Experiments Measuring Surfactant Self-Diffusion. Fluorescence recovery after photobleaching (FRAP) experiments are often used to measure fluorophore self-diffusion coefficients in adsorption layers, thin films, and lipid membranes.[19] We modified the fluorescence microscopy method to investigate the self-diffusion of pyrene derivatives in protein crystals. The experiments were performed on fluorescent orthorhombic lysozyme crystals after they had been equilibrated with the surfactant in the surrounding solution (typically after 48 h). The photobleaching was accomplished by switching to an objective with higher magnification, closing the field diaphragm to a minimum, and increasing the light intensity to a maximum by fully opening the illuminator aperture. Under these conditions, an intense bright spot of light was focused on a small area in the middle of the crystal. As the photostability of the pyrene is moderate, the excited molecules in the crystal irreversibly degraded to a nonfluorescent state and the intensity of the brightly fluorescent area decreased. After 20 min of intensive photobleaching the microscope was switched back to its usual low-magnification, low-power excitation mode and images of the crystal were taken at appropriate intervals.

The photobleaching procedure resulted in fluorescent crystals with darker bleached areas in the middle (Figure 8). The intensity measurements were made along the long axis of the crystals, i.e., horizontally in the middle of the crystal as shown in Figure 8. The data collected in this way are sensitive only to the lateral self-diffusion of the surfactant and would not be affected by additional infusion from the crystal boundaries, which may change the background intensity, but not the difference between the bleached and nonbleached areas. The image data were averaged over vertical columns 15 pixels high

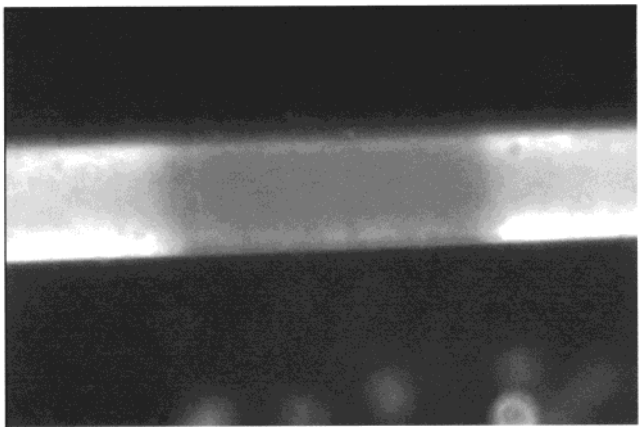

Figure 8. Fluorescence picture of a lysozyme crystal saturated with P-80 and then photobleached in the central area.

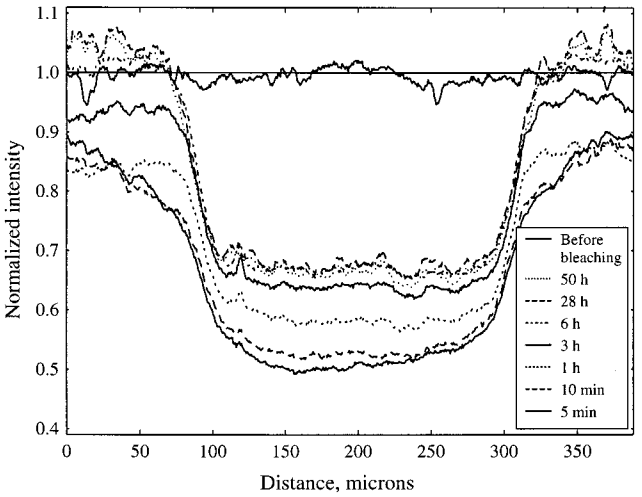

Figure 9. Intensity curves vs time along a photobleached area in a crystal similar to that in Figure 8. The lack of smearing and leveling off in the boundaries surrounding the bleached area in the center indicates that surfactant self-diffusion is either extremely slow or not present at all.

and corrected for the intensity profile of the excitation source (obtained over the uniformly bright crystal before photobleaching). Figure 9 shows the results from a typical experiment with P-80. The profiles were not normalized with respect to the background intensity and so show a generally uniform increase of the intensity levels in time. What is important, however, is that the *shapes* of the intensity profiles through the photobleached area and the depth of the darker "well" do not change significantly with time, even after periods as long as 50 h. Similar photobleaching results were also obtained with the carboxylic acid derivatives P-1903 and P-3840. This means that there is no exchange between the surfactant molecules in the bleached and unbleached areas in the crystal, and the effective

self-diffusion coefficient is negligible. Thus the self-diffusion coefficient (measured by FRAP) is even lower than the already small gradient diffusion coefficient (measured by the infusion technique); this trend is the same as that for diffusion coefficients in solution, although for the effective coefficients in the present case this may not have been predicted because of the added complexity engendered by the coupling with adsorption. In any event, the practical implication is that once the crystal is saturated with surfactant, the adsorbed molecules remain effectively immobilized on the protein matrix.

Discussion

Interaction between Protein Crystalline Matrices and Surfactants. The crystalline protein matrix is an effective substrate for surface-active and hydrophobic molecules. Values for the energy of interaction between anionic surfactants and lysozyme in solution have been reported by Jones and Manley.[5] The measured energies of binding of one or two molecules of surfactant to a molecule of lysozyme at pH 9 were found to be 8.2 *kT* for sodium decyl sulfate and 9.8 *kT* for sodium dodecyl sulfate. These compare well with the value of approximately 10 *kT* reported here, since our molecules have larger hydrocarbon portions and will exhibit stronger hydrophobic attraction to the protein. Thus the energy of surfactant adsorption onto proteins in a crystal appears to be similar to that for proteins in solution.

The strength of the interaction seems to be affected by the type and the size of the surfactant side chain, as demonstrated by the data at pH 10. For the carboxylic acids, the increase in length of the side chain from C_1 to C_3 leads to a 3-fold decrease of the diffusivity, which corresponds to an increase in the adsorption energy of about 1 *kT*. This may be explained by the increased flexibility of the side chain, which could allow the hydrophobic and the hydrophilic parts of the molecule to adopt more optimal configurations in a binding event. A further increase in the length of the side chain from C_3 to C_5 leads to decreased solubility, as expressed by differing values of I_0 in solution, but no significant changes in the adsorption energy were detected.

The replacement of the carboxylic acid by sulfonate causes a small change in the diffusivity and adsorption energy, while the lowest mobility and hence the highest adsorption energy were measured with the 1-pyrene propylamine. Unlike the other surfactants, the amine group is likely to be positively charged at pH 10,[20] and since the protein is positively charged here as well, the stronger adsorption is surprising. A possible explanation lies in the nature of the crystal contacts in orthorhombic lysozyme calculated from the crystallographic coordinates[18] based on a criterion of interatomic distances <4.5 Å: 10 of the 11 Arg and 2 of the 6 Lys residues are involved in contacts, vs only 4 of the 7 Asp and neither of the Glu residues. Thus, although the net charge on lysozyme is positive, many of the positive charges that provide likely sites for anions are in fact buried, while the negative charges are largely accessible to solvent.

The situation changes substantially in the case of the (tetragonal) protein crystals at pH 6.5. The mobilities of both pyrene butanoic acid and pyrene butylamine are much higher in these crystals than in the ones at pH 10. This can, to a certain extent, be attributed to the different orientation of the molecules and size of the channels in the tetragonal crystal compared to the orthorhombic one. However, as the volume per molecule in both crystals is approximately the same, it appears more likely that the observed difference is related to the charge state of lysozyme at pH 6.5. The net charge of lysozyme can be estimated from the pK_as of the ionizable amino acid residues to be about $+4$ at pH 10 and about $+8$ at pH 6.5, and furthermore, only 7 Arg and 2 Lys residues are involved in contacts.[18] The higher charge of lysozyme and greater accessibility of the basic residues will increase repulsion of positively charged surfactants, as is apparently confirmed by the diffusivity and adsorption energies of P-1903 (carboxylic acid) and P-6254 (amine). Both surfactants are more mobile at pH 6.5 than at pH 10, but while the amine is adsorbed more strongly at pH 10, it is adsorbed less strongly and is very mobile at pH 6.5. In summary, although hydrophobic interactions may certainly contribute to surfactant adsorption, our data suggest that the relative binding energies are determined largely by electrostatic interactions.

Crystallization and Material Science Aspects. Surfactants are often present during protein separation, purification, and characterization, either as impurities or as additives. Commercially isolated proteins may contain lipids, detergents, and peptides. Surfactants are sometimes added to enhance the crystallization of proteins for X-ray investigations, although the mechanism of their action is usually unknown. Our results show that crystallization may be an impractical method for purification of proteins from the above impurities, as the amphiphiles may be adsorbed and incorporated into the growing crystals, and the long time scales of their diffusion out of the matrix make washing them out practically infeasible. On the other hand, the use of surfactants during the washing and treatment of existing crystals may not lead to significant contamination of the protein, due to the slow infusion kinetics (in contrast to proteins in solution, where the adsorption is almost immediate). The results show the potentially interesting ability of protein crystals to collect, concentrate, and store low-solubility hydrophobic molecules from the surrounding solution. Thus, protein crystals or other dense phases may find applications as biocompatible carriers of drugs and active substances that either are of low solubility, or need to be released slowly.

This work also has interesting aspects related to the potential use of organized protein matrices in materials science applications. While the strength of adsorption of the surfactant molecules to protein molecules appears to be approximately the same in solution or in a crystal, the collective properties of the crystalline matrix have important implications. The surfactants infuse the protein matrix due to concentration gradients across the crystal, but once these gradients have dissipated, the fluorescent molecules remain effectively immobile in the protein matrix.

The collective properties of the protein−surfactant lattice formed, or the spatially uniform distribution of the organized molecules, can be used in a variety of ways, such as light-triggered moieties for energy transfer, data storage, or micromanipulation. A very rudimentary example of such events is presented in Figures 5 and 8. Some further aspects of photomanipulation of the fluorophore-infused crystals that we have studied have been presented separately.[12] An interesting question related to the crystal infusion is whether the surfactant molecules in the saturated crystal are organized in any ordered structure, or oriented in a few preferred configurations. We have carried out preliminary X-ray characterization studies of our lysozyme-infused crystals and have found no ordered surfactant molecules in the resolved structure at a resolution as high as 1.6 Å.[9] Thus the amphiphile is not adsorbed in an ordered fashion or preferred location on the surface of the protein. This validates our model assumption that there is no specific binding of the adsorbed amphiphiles.

Concluding Remarks

The new method reported here allows characterization of protein−surfactant interactions inside crystalline protein matrices, based on quantitative measurement of the rate of fluorescent surfactant infusion and self-diffusion. We have shown that the surfactants either can be incorporated into growing protein crystals or can penetrate and adsorb afterward. The measured diffusion coefficient of the surfactant in a crystal is about 10^3 times lower than that in solution, which corresponds to an adsorption energy of about 10 *k*T, close to that in solution. After saturation the amphiphiles appear to be firmly immobilized in the protein matrix. The results can find application in at least two directions. First, the data and methods may be used in optimizing protein−surfactant coupling for protein crystallization. Second, we believe that the fluorescence infusion method described here has promise for further investigation of surfactant−protein or substrate−protein interactions in condensed phases, including not only crystals, but also precipitates and gels. The method can potentially be used to probe the structure and permeability of complex three-dimensional polypeptide networks.

Acknowledgment. This study was supported by NASA (grant NAG8-1346).

References and Notes

(1) Durbin, S. D.; Feher. G. *Annu. Rev. Phys. Chem.* **1996**, *47*, 171.

(2) (a) George, A.; Wilson, W. *Acta Crystallogr*. **1994**, *D50*, 361. (b) George, A.; Chiang, Y.; Guo, B.; Arabshahi, A.; Cai, Z.; Wilson, W. W. *Methods Enzymol.* **1997**, *276*, 100. (c) Neal, B. L.; Asthagiri, D.; Velev, O. D.; Lenhoff, A. M.; Kaler, E. W. *J. Cryst. Growth*, **1998**, *196*, 377.

(3) (a) Muschol, M.; Rosenberger. F. *J. Chem. Phys.* **1995**, *107*, 1953. (b) Velev, O. D.; Kaler, E. W.; Lenhoff, A. M. *Biophys. J.* **1998**, *75*, 2682.

(4) Only the crystallization of soluble proteins is studied here. Membrane proteins, which are usually solubilized with surfactants (for a review see, e.g., Kühlbrandt, W. *Q. Rev. Biophys.* **1988**, *21*, 429), are not discussed.

(5) Jones, M. N.; Manley, P. *J. Chem. Soc., Faraday Trans. I* **1979**, *75*, 1736.

(6) (a) Fukushima, K.; Murata, Y.; Nishikido, N.; Sugihara, G.; Tanaka M. *Bull. Chem. Soc. Jpn.* **1981**, *54*, 3122. (b) Turro, N. J.; Lei, X.-G.; Ananthapadmanabhan, K. P.; Aronson, M. *Langmuir* **1995**, *11*, 2525.

(7) (a) McPherson, A.; Koszelak, S.; Axelrod, H.; Day, J.; Robinson, L.; McGrath, M.; Williams, R.; Cascio, D. *J. Cryst. Growth* **1986**, *76*, 547. (b) McPherson, A.; Koszelak, S.; Axelrod, H.; Day, J.; Robinson, L.; McGrath, M.; Williams, R.; Cascio, D. *J. Biol. Chem.* **1986**, *261*, 1969. (c) Mustafa, A. O.; Derrick, J. P.; Tiddy, G. J. T.; Ford, R. C. *Acta Crystallogr.* **1998**, *D54*, 154.

(8) (a) Moren, A. K.; Khan, A. *Langmuir* **1995**, *11*, 3636. (b) Moren, A. K.; Khan, A. *Langmuir* **1998**, *14*, 6818.

(9) Velev, O. D.; Pan, Y.; Kaler E. W.; Lenhoff, A. M., manuscript in preparation.

(10) Lakowicz, J. R. *Principles of Fluorescence Spectroscopy*; Plenum Press: New York, 1983; pp 341−381.

(11) (a) Alderton, G.; Ward, W. H.; Fevold, H. L. *J. Biol. Chem.* **1945**, *157*, 43. (b) Artymiuk, P. J.; Blake, C. C. F.; Rice, D. W.; Wilson, K. S. *Acta Crystallogr.* **1982**, *B38*, 778.

(12) The protein is probably denatured by a process of energy transfer from the pyrene derivatives to the host lysozyme molecules, leading to denaturation and eventual fragmentation. An enlightening study of analogous photochemical splicing of lysozyme in solution by pyrenes has been described recently by: Kumar, C. V.; Buranaprapuk, A.; Opiteck, G. J.; Moyer, M. B.; Jockusch, S.; Turro, N. J. *Proc. Natl. Acad. Sci. U.S.A.* **1998**, *95*, 10361. This phenomenon can be used for micromachining of protein crystals: Velev, O. D.; Kaler, E. W.; Lenhoff, A. M. *Adv. Mater.* **1999**, *11*, 1345.

(13) (a) Satterfield, C. N. *Mass Transfer in Heterogeneous Catalysis*; MIT Press: Cambridge, MA, 1970. (b) Deen, W. M. *AIChE J.* **1984**, *33*, 1409.

(14) Vieth, W. R. *Diffusion in and through Polymers: Principles and Applications*; Oxford University Press: New York, 1991.

(15) Carslaw H. S.; Jaeger, J. C. *Conduction of Heat in Solids*; Oxford University Press: New York, 1986.

(16) Crank, J. *The Mathematics of Diffusion*; Clarendon Press: Oxford, UK, 1979.

(17) Perry, R. H., Green, D. W., Maloney, J. O., Eds.; *Perry's Chemical Engineering Handbook*; McGraw-Hill Publ.: New York, 1984; Sect. 3, pp 258−291.

(18) The following files from the Brookhaven Protein Data Bank were used: 1AKI (orthorhombic) and 6LYZ (tetragonal).

(19) See for example: Koppel, D. E. In *Fast Methods in Physical Biochemistry and Cell Biology*; Sha'afi, R. I., Fernandez, S. M., Eds.; Elsevier: New York, 1983; pp 339−367. Edidin, M. In *Mobility and Proximity in Biological Membranes*; Damjanovich, S., Szöllosi, J., Tron, L., Edidin, M., Eds.; CRC Press: Boca Raton, FL, 1994; pp 109−135.

(20) The pK_a value should be similar to that of propylamine, viz., ca. 10.7: *CRC Handbook of Chemistry and Physics*; Weast, R. C., Ed.; CRC Press: Boca Raton, FL, 1995.